Early diagnosis of oral cancer based on the surface plasmon resonance of gold nanoparticles

James Chen Yong Kah[1]
Kiang Wei Kho[2]
Caroline Guat Leng Lee[2]
Colin James Richard Sheppard[1]
Ze Xiang Shen[3]
Khee Chee Soo[2]
Malini Carolene Olivo[2]

[1]Division of Bioengineering, National University of Singapore, Singapore; [2]Division of Medical Sciences, National Cancer Centre Singapore, Singapore; [3]School of Physical and Mathematical Sciences, Nanyang Technological University, Singapore

Abstract: The high mortality rate in cancer such as oral squamous cell carcinoma is commonly attributed to the difficulties in detecting the disease at an early treatable stage. In this study, we exploited the ability of gold nanoparticles to undergo coupled surface plasmon resonance and set up strong electric fields when closely-spaced to improve the molecular contrast signal in reflectance-based imaging and also to enhance the Raman signal of bioanalytes in cancer. Colloidal gold nanoparticles were synthesized and conjugated to anti-epidermal growth factor receptor (EGFR) for imaging. A self-assembled surface enhanced Raman scattering (SERS)-active gold nanoparticle monolayer film was also developed as a biosensing surface using a simple drop-dry approach. We have shown that gold nanoparticles could elicit an optical contrast to discriminate between cancerous and normal cells and their conjugation with antibodies allowed them to map the expression of relevant biomarkers for molecular imaging under confocal reflectance microscopy. We have also shown that the SERS spectra of saliva from the closely-packed gold nanoparticles films was differentiable between those acquired from normal individuals and oral cancer patients, thus showing promise of a simple SERS-based saliva assay for early diagnosis of oral cancer.

Keywords: Gold nanoparticles, reflectance imaging, confocal microscopy, epithelial carcinoma, epidermal growth factor receptor, coupled surface plasmon resonance, oral cancer, surface enhanced Raman scattering

Introduction

Oral squamous cell carcinoma is the sixth most common cancer for both sexes worldwide. The 5-year survival rate of the disea0se is currently about 50%. Oral cancer is often diagnosed only after it has advanced to an untreatable stage (Spafford et al 2001; Zheng et al 2002) where the cancer cells have become aggressive and immune to therapeutic drugs. Detecting oral cancer at its earliest is thus vital for improving the survival rate of this disease. Current clinical diagnosis of most epithelial cancers, including oral cancer, typically involves performing invasive needle biopsies followed by histological examination on the excised tissue. The procedure may present psychological trauma and risk of infection to patients. Furthermore, biopsy is usually performed only under the condition that the lesions are spotted and appear abnormal (Lumerman et al 1995). Yet, pre-cancerous lesions can appear innocuous or occur in hidden sites such as the crypts in the base of tongue, and can therefore easily go undetected even with white-light endoscopy (Spafford et al 2001). Furthermore, conventional histopathological diagnosis is based on morphological and structural changes at the cellular or tissue level, which may not be obvious for early-stage tumors (Wickline and Lanza 2000). Taken together, it is clear that a diagnostic method for detecting early stage oral cancer is highly desired.

Recently, an increased amount of efforts has been made to develop less-invasive early diagnostic modalities for oral cancer, of which the in vivo high resolution imaging of oral epithelial tissues using novel optical systems (Sokolov, Aaron et al 2003)

Correspondence: Malini Carolene Olivo
Division of Medical Sciences, National Cancer Centre Singapore, 11 Hospital Drive, Singapore 169610
Tel +65 64368317
Fax +65 63720161
Email dmsmcd@nccs.com.sg

and the chemical analysis of saliva (Chen et al 2002) hold great promises as valuable tools. However, these techniques are met with several limitations to their effective use as diagnostic tools. Although advanced optical systems for *in vivo* imaging such as optical coherence tomography (OCT) and confocal reflectance endomicroscopy are designed to image cell and stromal morphology for non-invasive clinical diagnosis in real time, the contrast between neoplastic and normal tissues is often too low to be of any clinical value (Wickline and Lanza 2002). Furthermore, these structural-based imaging techniques are unable to image the biomolecular changes associated with carcinogenesis *in vivo* (Koenig et al 2001) due to their inherent optical configurations, which can provide earlier and more accurate diagnosis for suspicious pre-cancerous lesions as compared to their structural and morphological changes.

Although these biomolecular changes can potentially be detected through non-invasive quantitative assessment of the chemical compositions of saliva (Chen et al 2002) using techniques such as enzyme-linked immunosorbent assay (ELISA), micro-satellite analysis and high performance liquid chromatography (HPLC), these highly specific techniques in molecular detection are usually labor-intensive procedures and requires long analysis time. Even as this can be overcome substantially using mass spectrometry (MS), which normally gives a shorter analysis time and higher sensitivity, a clinically reliable MS data for saliva specimens is unfortunately hard to come by because issues such as ion-suppression effect, non-universal ionization efficiency, and machine-to-machine variations, have complicated MS analysis of such complex sample as saliva (Li et al 2001). Furthermore, these techniques have yet to discover reliable and well-validated markers for oral cancer. Raman spectroscopy is another technique that has long been used to study cancer-related chemical changes in both cancerous tissues as well as bio-fluids. For instance, Li et al has shown that the Raman spectra of sera collected from normal individuals and cancer patients are different in more than 80% of cases for various cancers (Li et al 2001). However, the Raman signals from these biologic samples are usually weak and not sensitive enough to merit clinical value.

Gold nanoparticles have recently been investigated to address the limitations of these imaging and chemical-based diagnostic techniques based on their optical properties. These metallic nanoparticles exhibit unique optical response to light which allow them to resonantly scatter light when excited at their surface plasmon resonance frequency (Mulvaney 1996). Furthermore, the scattering cross section per particle is increased when the gold nanoparticles aggregate to produce an even larger optical signal (Sokolov, Follen et al 2003). This mode of enhanced scattering from coupled surface plasmon resonances of aggregated gold nanoparticles can be exploited to provide good optical contrast if the gold nanoparticles can be brought close together in cellular environment under the influence of biochemical processes associated with disease pathology. As such, gold nanoparticles show potential as optical probes for reflectance-based optical imaging to address their limitation in providing contrast for early biomolecular signatures present in cells and tissue (Schultz et al 2000; Sokolov, Follen et al 2003; El-Sayed et al 2005). Furthermore, when the gold nanoparticles are closely-packed to form a film, they are also capable of undergoing plasmon resonance with the laser excitation wavelength to generate strong excitation fields on the film surface and this can be used to improve the sensitivity of optical based Raman spectroscopy for the chemical analysis of diluted fluid analytes such as saliva specimen applied on its surface.

Gold nanoparticles also possess other favorable physicochemical properties for use as optical probes for early diagnostics. They can be easily conjugated to antibodies or peptides through electrostatic charge interaction or coordinate bonding to probe for specific cellular biomarkers with high specificity and affinity (Geoghegan and Ackerman 1977). When coupled with appropriate biomarkers, these gold nanoparticles bioconjugates may provide useful optical signal for molecular specific information to assist clinicians in diagnosis of pre-cancers. Gold nanoparticles are also generally biocompatible and benign in biological tissues and have been applied for clinical treatment of other disease conditions such as rheumatoid arthritis (Abrams and Murrer 1993).

In this study, our objectives were to develop colloidal gold nanoparticles as well as a self-assembled monolayer of these nanoparticles and exploit their ability to undergo coupled surface plasmon resonance and set up strong electric fields when closely-spaced for cancer diagnosis using both an imaging and chemical approach. Under the imaging approach, we demonstrated the use of these nanoparticles as an optical contrast agent for improving the optical contrast of clinically relevant biomarkers in epithelial cancer cells under reflectance-mode imaging *in vitro*. The epidermal growth factor receptor (EGFR) is one such clinically relevant cell surface receptor biomarker used in this study that is overexpressed in vast majority of epithelial cancer but not in normal cells (Eisbruch et al 1987; Shin et al 1994; Ke et al 1998; Nouri et al 2000). Under the chemical approach, we demonstrated the use of gold nanoparticles in surface enhanced Ra-

man scattering (SERS) to enhance the Raman spectroscopy signal for the analysis of cancer-related chemical changes in saliva. We developed a simple and cost-effective method for preparing highly sensitive SERS-based saliva assay based on SERS-active gold nanoparticle films and used it to collect and analyze spectroscopically, the SERS from the sample-film interface to seek for spectral features indicative of oral cancer. The use of saliva as a diagnostic fluid would offer a few advantages over previous sera-based counterparts in that saliva is easily accessible, painlessly acquired and presents lower risk of infection compared to serum.

Materials and methods

Synthesis and characterization of gold nanoparticles

Colloidal gold nanoparticles were synthesized by the reduction of 0.259 mM of hydrogen tetrachloroaurate (Sigma-Aldrich) by 34 mM of trisodium citrate (Sigma-Aldrich) at temperature of 90 °C (Hayat 1989). The particle size was determined by transmission electron microscopy (TEM) (Jeol JEM-1010 100 kV) to show uniform spherical and monodisperse gold nanoparticles with an average diameter of 15 nm. Their UV-Vis extinction spectrum was characterized using a UV-Vis spectrophotometer (Shimadzu UV-2401 PC). The side-scatter spectrum of the gold nanoparticles was characterized using a USB2000 miniature fiber optic spectrophotometer (Ocean Optics, Inc) by illuminating the colloidal sample and detecting the spectrum at 90° to the incident illumination. The concentration of the gold nanoparticles in the colloid was characterized against known gold hydrosol standards from British Biocell International Ltd (EMGC.15, particle concentration = 1.4×10^{12} particles per ml) and was determined to be approximately 1.23×10^{12} particles per ml. This colloid was stored at 4 °C when not used.

SERS substrate preparation and characterization

SuperFrost®Plus microscope glass slides (VWR Scientific) were rinsed thoroughly with 70% v/v aqueous solution of ethanol (Merck) for 1 minute. The slides were then rinsed four times to remove traces of ethanol with fresh distilled water (18 MΩ, obtained from Millipore Mili-Q water purification system) each time. The slides were stored in water until needed. To fabricate a gold particle film, a 150-µl droplet of gold nanoparticles was pipetted onto the surface of a cleaned slide. The slide was then dried in a dessicator for 24 h, followed by rinsing in distilled water, after which the slides were dried with a dust blower. All of the prepared gold colloid films were kept in distilled water until needed.

Optical transmission measurements of the resultant gold colloid films were performed using a Shimadzu UV-2401 PC monochromator system. A cleaned SuperFrost®Plus microscope slide was used as the reference sample. Each slide bearing a gold film was placed in the illumination light path and secured with blue-tack. The light beam was passing through the slide perpendicularly. Care was taken to ensure that the blue-tack was not in the light path. Atomic force microscopy (AFM) measurements were performed under ambient conditions using a Digital Instrument DI3000 Nanoscope III in tapping mode (247.9 KHz) with a typical resolution of about 5 to 15 nm, and a horizontal scanning rate of 1 Hz.

Conjugation of gold nanoparticles with anti-EGFR

The gold nanoparticles were conjugated to monoclonal anti-EGFR (Santa Cruz Biotechnology Inc.) as our selected cancer biomarker for imaging via established protocols for passive absorption of anti-EGFR on the surface of gold nanoparticles. Briefly, the conjugation was performed by incubating the gold nanoparticles with anti-EGFR for about 10 mins at room temperature as according to a modified procedure reported previously (Geoghegan and Ackerman 1977). The successful conjugation of antibodies on gold nanoparticles was ascertained by addition of 10% common salt solution and observing any visible color change in the colloidal solution. The presence of salt caused unconjugated gold nanoparticles to aggregate and result in a visible color change from red to purple or gray. After the 10 minutes of incubation time, the anti-EGFR conjugated gold nanoparticles were washed and resuspended in 1X PBS buffer (pH 7.4) containing 5% bovine serum albumin (BSA) (Sigma Aldrich, Inc) and stored at 4 °C. Spectrophotometry was performed using the same Shimadzu UV-2401 PC monochromator system to confirm conjugation of anti-EGFR to gold nanoparticles. The gold nanoparticles were also conjugated to BSA, a non-cellular binding protein, as negative control probes using the same procedures as above.

Cellular imaging

Both the poorly-differentiated nasopharyngeal epithelium carcinoma CNE2 cell line and the normal human lung fibroblast (NHLF) cell line were used in this study. The CNE2 cells were grown in RPMI 1640 supplemented with 10% fetal bovine serum, 2 mM glutamine, sodium pyruvate,

non-essential amino acids and 100 unit/ml penicillin/streptomycin while the normal cells were grown in fibroblast growth medium (Cambrex Corp.). Both cell lines were grown and maintained at 37 °C in humidified 5% CO_2 and 95% air atmosphere. Prior to imaging, both cell lines were trypsinized and fixed in 2% paraformaldehyde before incubating them with the anti-EGFR conjugated gold nanoparticles for 2 h at 37 °C. The cells were also incubated with BSA conjugated gold nanoparticles as a negative control for the antibody binding. Following the incubation, the cells were rinsed thrice with PBS to wash away the excess and unbounded gold bioconjugates and were then placed on a microscope slide for imaging. Imaging was performed using a confocal microscopy (LSM510 Meta, Carl Zeiss) in the reflectance mode with a 20X olympus objective under 633 nm excitation with a helium-neon laser.

Preparation of saliva samples

Saliva samples were collected from 5 normal healthy individuals and 5 oral-cancer patients following their informed consent. This study was reviewed and approved by the Ethics Committee of the National Cancer Centre Singapore. Each subject was asked to rinse their mouth thoroughly with water for 30 min to remove any food particles in their oral environment, before expelling saliva into a 15 ml plastic container (Nalgene, Eppendorf). About 1 ml of whole saliva was obtained each time. The specimen was then transferred into a 1.5 ml Eppendorf centrifuge tube and spun, using the Eppendorf Centrifuge 5415C, at 14,000 rpm for 5 min to remove small particulates and exfoliated cells. The supernatant was then extracted and stored in a new centrifuge tube at –20 °C until needed. Note that only samples with no sign of blood contamination are used for the experiment.

SERS measurements

The Raman experiments were carried out with a modified micro-Raman system, in which an Olympus microscope with a color closed circuit television (CCTV) system was coupled to a Spex 1704 spectrometer that was equipped with a liquid nitrogen cooled CCD detector. In this modified system, the coupling optics was arranged in a box that was linked to the modified optical microscope by a mechanical arm and fixed to the Spex spectrometer. The laser light at 632.8 nm was introduced from the back of the box, after passing through a plasma filter and was then directed into the modified microscope via a notch filter. This notch filter acted as a reflection mirror to the laser light, but to the signal returning from the sample, it was a very effective filter to the Rayleigh (laser) line. This filter prevented any backscattered laser from entering the spectrometer, and hence from interfering with the Raman signals to be collected, but allowed Raman signals to transmit with little attenuation. The returned signals then passed through a second notch filter which was used to further improve the Rayleigh rejection. The Raman signal was then focused onto the entrance slit of the Spex spectrometer by a coated singlet focusing lens of 50 mm focal length. The inclusion of the CCTV system allowed both the laser beam and white light to be viewed directly from the monitor. A biological specimen could also be viewed directly from the monitor. The objective lens used in this study was from Olympus with magnification 10 × and NA 0.25. The closely-packed gold particle film was first coated with a drop (approximately 30 µl) of saliva. Immediately, a 633 nm laser was focused, via a 10 × NA 0.25 objective, onto the sample-film interface. Laser intensity at sample is about 2 mW. Spectrum acquisition was then started immediately. The spectral resolution was 1 cm^{-1} and an integration time of 10 s was used for all Raman measurements.

Results

The extinction and side-scatter spectrum of the gold nanoparticles is shown in Figure 1. The extinction spectrum (Figure 1a) shows a sharp peak at 520 nm which corresponds to the surface plasmon resonance typical of gold nanoparticles of that size (Murillo et al 2002). The side-scatter spectrum (Figure 1b) shows that the gold nanoparticles have the potential to scatter light strongly at around 600 nm. Since the light scattering of biological tissue in this wavelength range is small compared to the light scattering afforded by gold nanoparticles (Taroni et al 2003), the presence of the gold nanoparticles in tissue may be distinguishable from the scattering intensity. Spectrophotometry was used to confirm the conjugation of anti-EGFR to gold nanoparticles. The extinction spectrum of the gold nanoparticles both before and after conjugation with anti-EGFR was measured and is shown in Figure 2. The UV-Visible extinction spectrum shows a characteristic red-shift (≈6 nm) of the peak of the surface plasmon resonance which is typical of protein binding on the surface of the gold nanoparticles. This indicates the successful conjugation of anti-EGFR on the gold nanoparticles. An additional indication of anti-EGFR binding to the surface of the nanoparticles is their stability in 10% common salt solution where the gold bioconjugates did not aggregate to result in a color change after the addition of salt solution. The reduction in the intensity of the peak after conjugation

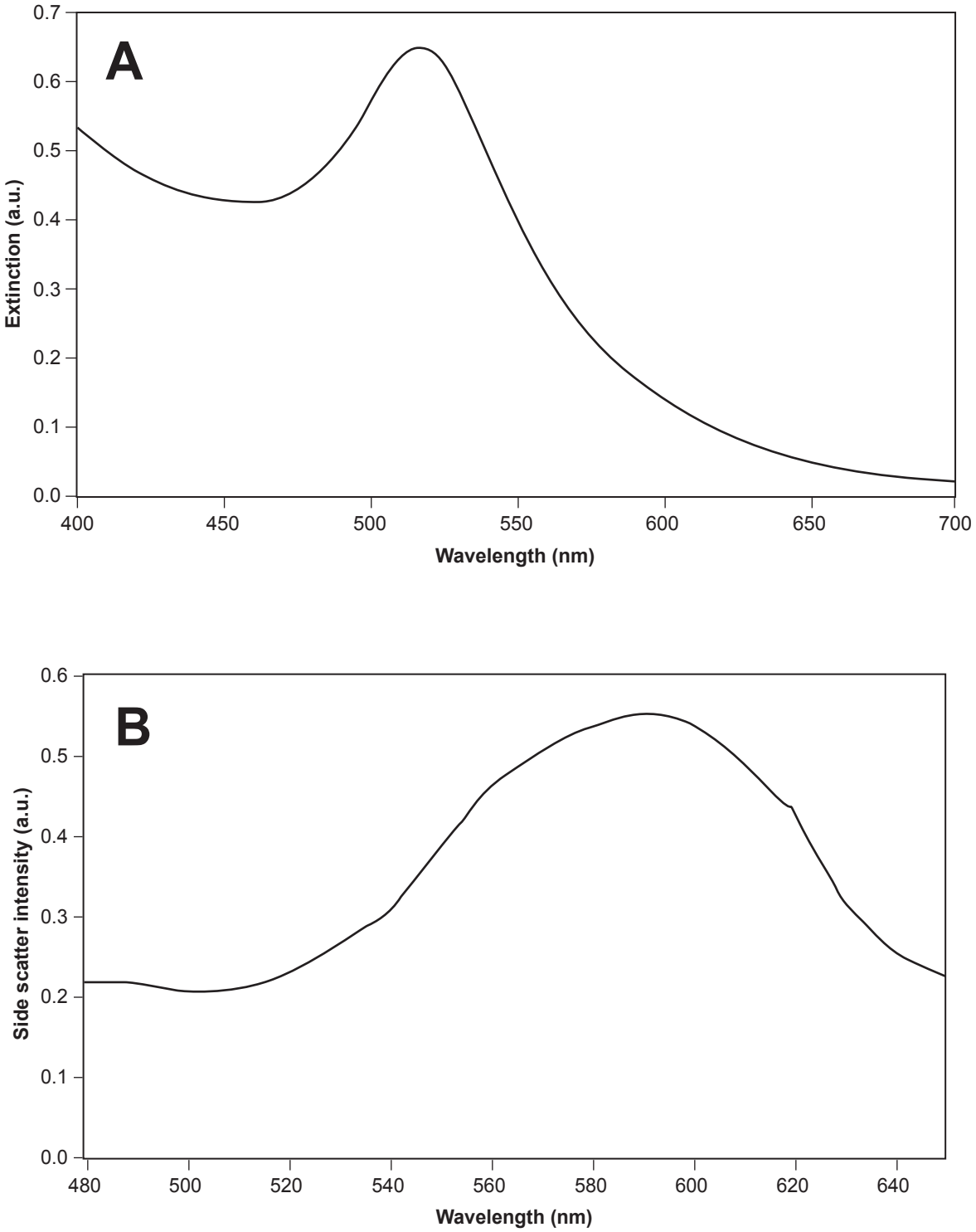

Figure 1 (**a**) Extinction spectrum of synthesized 15 nm gold nanoparticles with a peak plasmon resonance wavelength of 520 nm and (**b**) their side-scatter spectrum showing a peak reflectance of the gold nanoparticles at around 600 nm.

could be due to the loss in some gold nanoshells during the washing steps after conjugation.

The ability of gold nanoparticles to increase the optical scattering of cells when attached to their surface was investigated by labeling the cells with these nanoparticles and observing them under confocal reflectance microscopy. Figure 3 shows the confocal reflectance images of CNE2 cells before and after labeling with anti-EGFR conjugated gold nanoparticles, as well as CNE2 cells labeled with our control of BSA conjugated gold nanoparticles which are not known

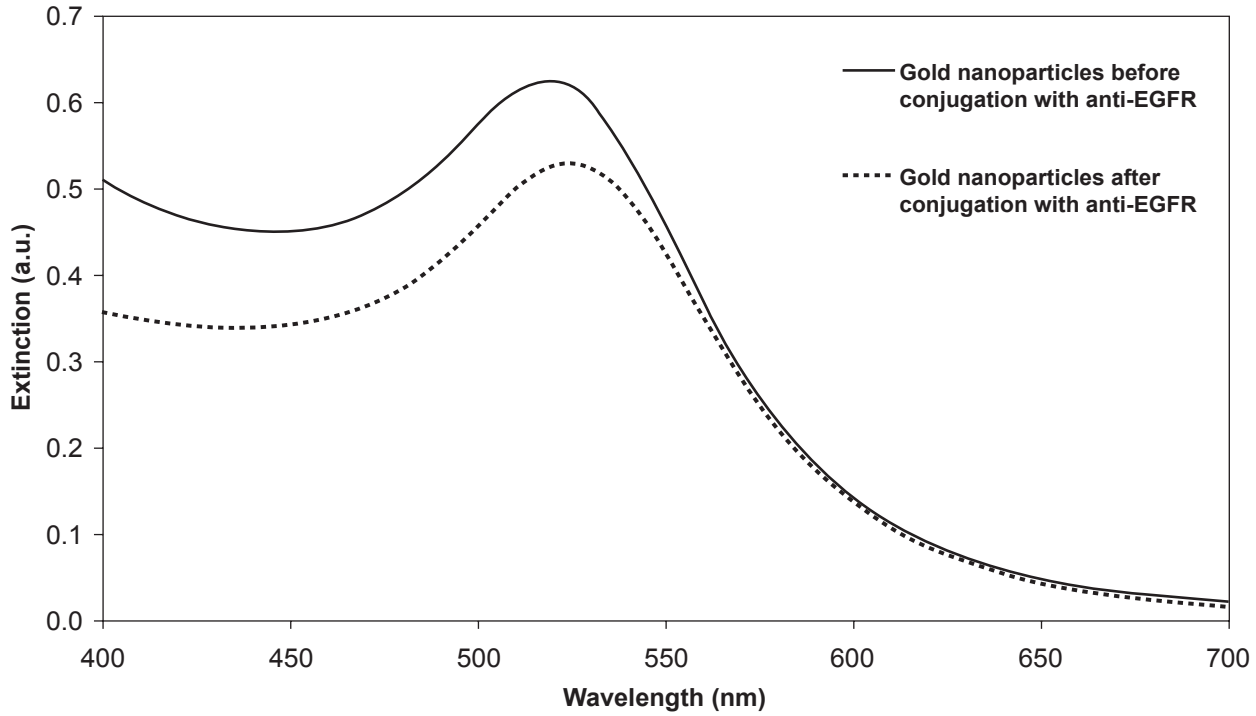

Figure 2 Changes in extinction spectrum of gold nanoparticles after conjugation with anti-EGFR to demonstrate the binding of anti-EGFR on gold nanoparticles. Spectrum after conjugation is shown in dashed line.

to exhibit high binding affinity to the cells. A significant increase in the reflectance signal was observed in the cells labeled with the antibody conjugated gold nanoparticles compared to the other two controls, where the reflectance signal seemed to be non-specific and at random and could barely be resolved from the dark background. The increase in reflectance signal that arose from the bright scattering ring formed could be attributed to the localization of the gold nanoparticles on the cell membrane as it was not observed in the unlabeled cells.

In addition to increasing the optical scattering on cells, the anti-EGFR conjugated gold nanoparticles also exhibited specificity in binding to cancer cells overexpressing EGFR compared to normal cells. The labeling of anti-EGFR gold nanoparticles on both CNE2 and NHLF cells under confocal reflectance microscopy is shown on Figure 4 together with their corresponding autofluorescence image. The autofluorescence images of the two cell lines show similar autofluorescence level. However, the overexpression of transmembrane EGFR in CNE2 cells caused more anti-EGFR

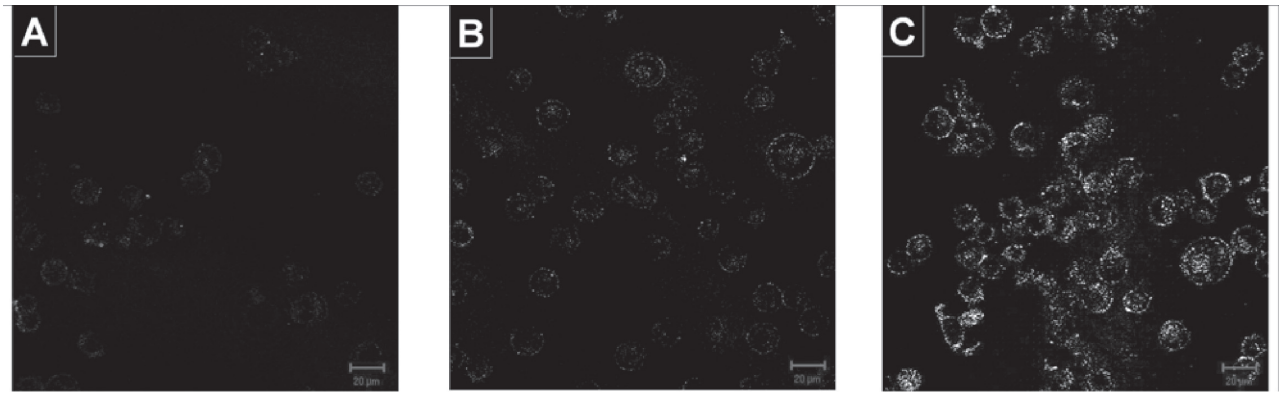

Figure 3 Confocal reflectance images of CNE2 cells (**a**) before labeling, (**b**) after labeling with our control BSA conjugated gold nanoparticles and (**c**) after labeling with anti-EGFR conjugated gold nanoparticles. Images are cross-sectional slices of cells taken at the mid-focal plane at 20X magnification. False-color reflectance images obtained at excitation 633 nm. Scale bar in all images is 20 μm.

gold nanoparticles to be selectively localized around the cytoplasmic membrane of the CNE2 cell compared to the nominal EGFR expression in normal NHLF cells, resulting in significantly higher reflectance intensity. The reflectance intensity of the CNE2 cells is about 30 times higher than that of the NHLF cells, sufficient to elicit an optical contrast between them for discriminating the cancerous against non-cancerous cells. As the regions of increased reflectance due to the presence of gold nanoparticles correspond to regions of high EGFR expression, this strong reflectance signal could provide a map of EGFR expression under confocal reflectance microscopy.

One of the objectives of this study was also to develop a simple and cost effective method for preparing SERS-active substrates which exploits the surface plasmon resonance of gold nanoparticles to enhance the Raman signal of bioanalytes. In particular, we looked at the fabrication of arrays consisting of closely spaced but non-aggregated monodisperse

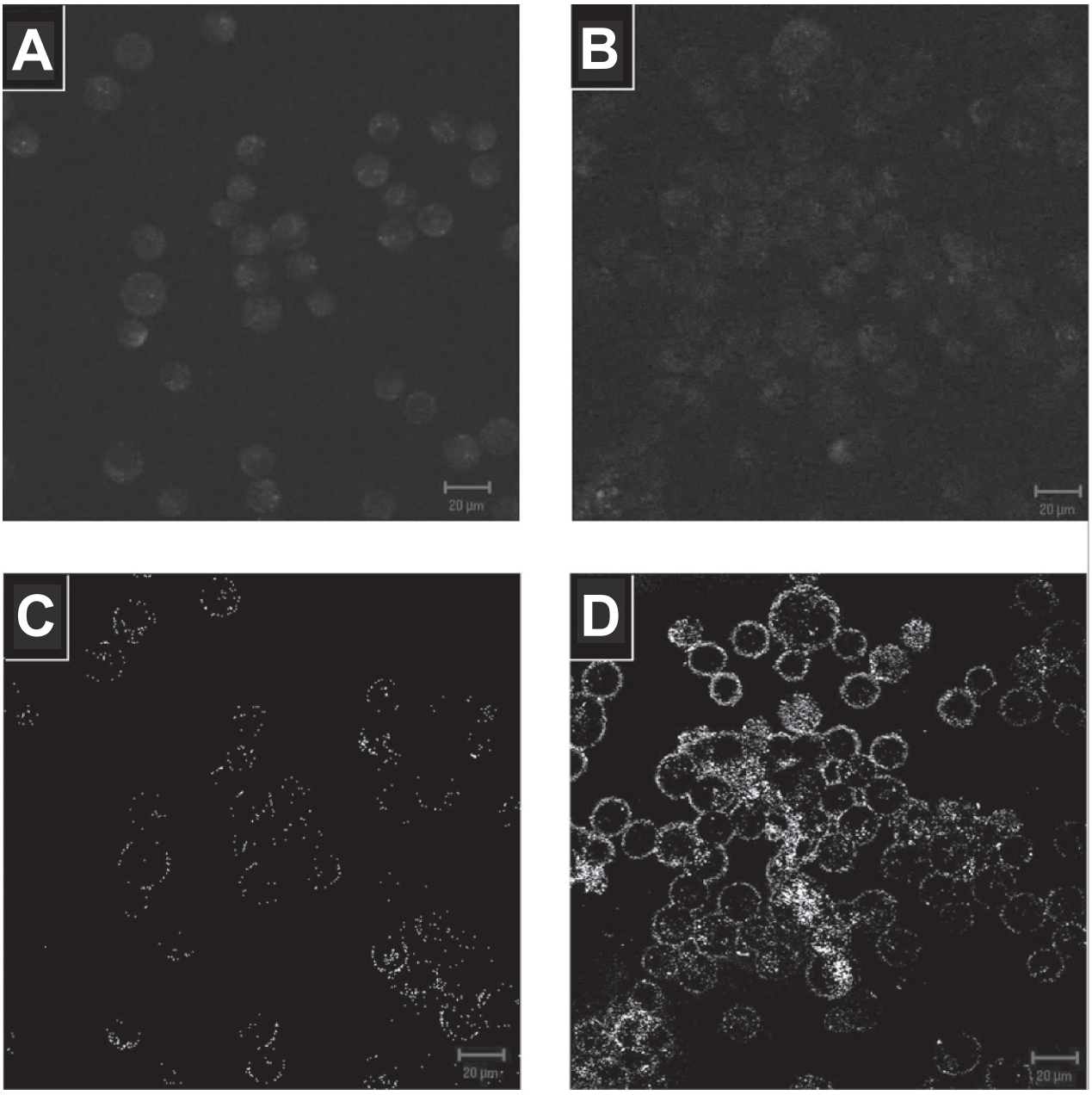

Figure 4 Autofluorescence image of (**a**) NHLF and (**b**) CNE2 cells. Their corresponding confocal reflectance images after labeling the (**c**) NHLF and (**d**) CNE2 cells with anti-EGFR gold nanoparticles is shown below the autofluorescence image. Images are cross-sectional slices of cells taken at the mid-focal plane at 20X magnification. False-color fluorescence images obtained at excitation 488 nm and reflectance images obtained at excitation 633 nm. Scale bar in all images is 20 µm.

nanoparticles, since it has been established by many previous studies that such an array could generate large SERS-activity (Katherine et al 1995). The large enhancement is derived mainly from the crevices between two adjacent particles, in which trapped analyte molecules experience enhanced electromagnetic field due to coupled surface plasmon resonance (Katherine et al 1995). Unfortunately, current techniques for preparing closely-spaced particle arrays are either too labour-intensive or too costly to scale up. As such, we have developed a simple alternative approach in which closely-packed arrays of metallic nanoparticle films were fabricated using a simple drop-dry approach. Figure 5 shows a SuperFrost®Plus microscope slide bearing three colloid films deposited by drying three 150-µl drops of gold nanoparticles containing 1.4×10^{12} particles per ml as delineated above. Each film is about 10 to 12 mm in diameter. Further observations under a microscope revealed interesting deposition pattern (see Figure 5b). Basically, three types of structures could be observed: a ring at the perimeter, a continuous layer (white arrow) and an unevenly coated region (dark arrow).

A representative UV-Vis spectrum of the gold nanoparticles film is shown in Figure 6, along with that of the gold nanoparticles colloid for comparison. One can immediately notice a double-peak feature in the film's spectrum (see curve A), which is an indication of a closely-packed but non-aggregated morphology, according to a previous computer simulation (Sanchez-Gil et al 2002). The first resonance peak in curve A situated at about 520 nm can be attributed to the plasmon resonance in the individual gold nanoparticles. The second peak located at 633 nm is derived from the collective plasmon oscillation among the closely-packed particles (Katherine et al 1995). Further analysis of the surface morphology was obtained from the AFM mapping of the uniformly coated regions. The result is shown in Figure 7. Analysis of the height profile revealed that the film was generally monolayer thick, with a small percentage of the total area being two- to three- particles thick.

Saliva samples were collected from 5 normal healthy individuals and 5 oral-cancer patients. Typical SERS spectra for these samples are shown in Figure 8. Tentative assignment of the major vibrational bands in the spectra based on existing knowledge is presented in Table 1. One of the differences between these spectra is the occurrence of Raman peaks at 670, 1097, and 1627 cm^{-1} in the abnormal-saliva spectrum (see bottom spectrum).

Table 1 Assignments of major vibrational bands in the SERS spectra of saliva samples

Observed raman shifts (cm^{-1})pp		Possible assignments
Normal	**Cancerous**	
432	432	Skeletal bending
493	–	
612	–	
–	670	υ (C–S)
709	–	υ (C–S) Met
–	1097	υ (C–N)
1114	–	υ (C–C)
1269	1269	δ (=CH) Phospholipid
–	1627	Trp, Tyr and Phe
1666–1700	1666–1700	Protein (Amide I): α -helix, β -sheet, random-coil

Discussion

The results of our study have demonstrated the exploitation of surface plasmon resonance of gold nanoparticles in performing cancer diagnosis through an imaging and a chemical analysis approach. We have synthesized and characterized the optical properties of 15 nm gold nanoparticles. The gold nanoparticles were conjugated to monoclonal anti-EGFR via passive absorption of the antibodies onto its surface and allowed to interact with cancer cells. The 6 nm red-shift in the peak surface plasmon resonance of the gold nanoparticles after conjugation with the antibody is associated with alterations in the local refractive index and hence dielectric constant around the surface of the gold nanoparticles particles due to the presence of a layer of antibodies around its surface. The change in dielectric constant affects the light scattering properties of gold nanoparticles according to the Mie theory (Bohren and Huffman 1983). This red-shift is typical of protein binding on the surface of the gold nanoparticles and serves as an indication of the presence of the antibodies on the surface of the gold nanoparticles.

The results of our in vitro experiments with the CNE2 cells have demonstrated that the anti-EGFR gold nanoparticles could serve as a potential optical contrast agent to increase the detection visibility of cells under reflectance-based imaging systems. The anti-EGFR were able to target and bind to the extracellular domain of EGFR on the cellular membrane even after conjugation to the gold nanoparticles. This means that the anti-EGFR still retains its antigen binding sites and activity after conjugation. The localization of the anti-EGFR gold nanoparticles forms highly reflective beacons due to the strong resonant light scattering response of gold nanoparticles on the cell surface to the excitation light. This resonant scattering condition is further enhanced when the gold nanoparticles cluster close together on the cell membrane as they attach to their receptor and their surface plasmon interacts with each other. This

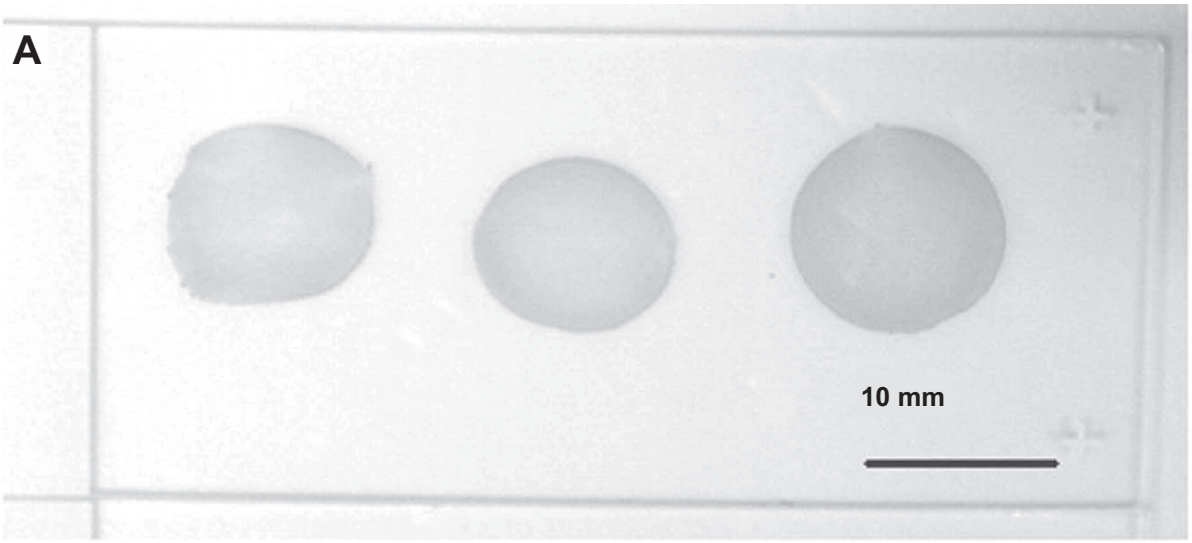

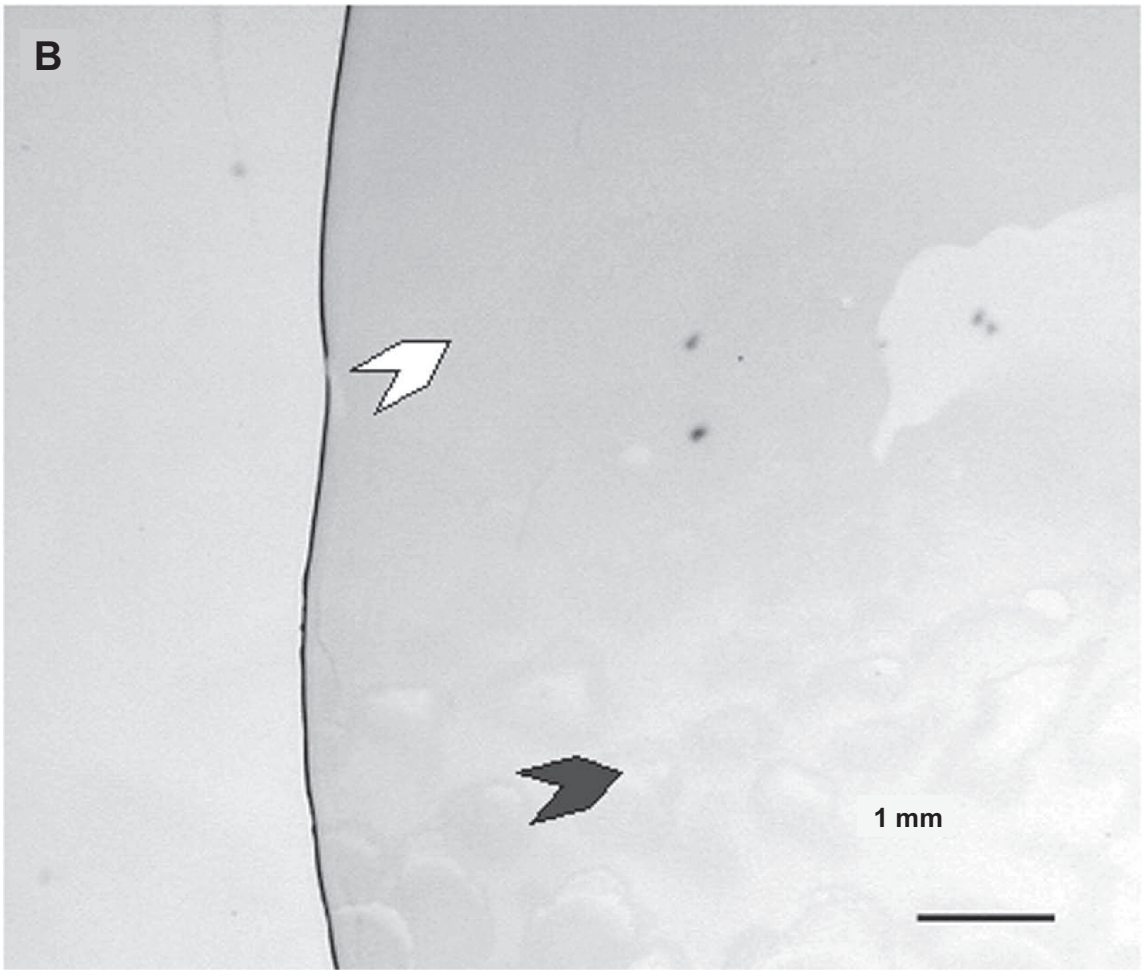

Figure 5 Macroscopic and microscopic images of colloid films by drying 150 μl of 15 nm gold nanoparticles on a SuperFrost®Plus microscope slide. (**a**) Macroscopic image of three colloid films. (**b**) Magnified view showing one fragment of a colloid film.

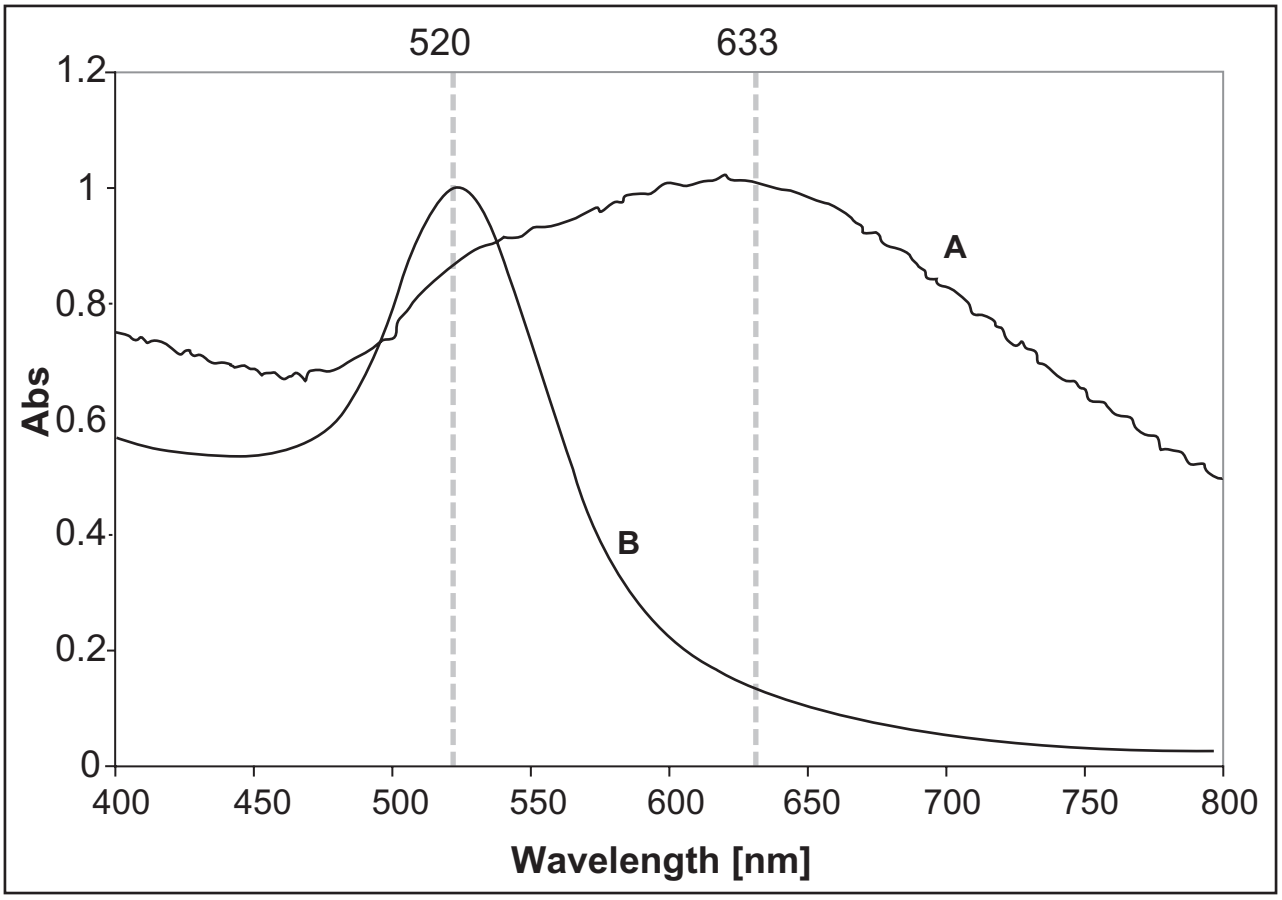

Figure 6 Normalized UV-Vis spectrum of a gold nanoparticles film obtained by drying a suspension droplet with an initial particle concentration of 1.4×10^{12} particles per ml (spectrum **A**) and the 15 nm colloidal gold nanoparticles (spectrum **B**).

result in bright reflectance rings being formed around the cytoplasmic membrane and their optical reflectance properties being increased significantly under confocal reflectance microscopy. In contrast, the strong reflectance signal from the bright scattering rings was not observed in our control labeling with a non-binding BSA conjugated gold nanoparticles as the BSA were unable to target and bind to the cells and were therefore removed during the washing steps after the incubation.

Furthermore, our results have also demonstrated the possibility of exploiting the strong optical response of gold nanoparticles to transduce the molecular signals into observable optical signals and generate molecular contrast to image the expression of EGFR in cancer cells. The gold labeling pattern arising from the increased in reflectance was able to provide a map of EGFR expression under confocal reflectance microscopy. However, as the nucleus and other organelles in the cells are also generally reflective (as depicted in Figure 4), we do note that the signal-to-noise ratio achieved using such reflective probe to image biomarker expression is generally lower than that achieved with fluorescent probes. Nonetheless, the reflectance signal from the gold nanoparticles probe should provide sufficiently high contrast against intrinsic reflectance signal in cells and tissue to map the biomarker expression under certain imaging application where the use of fluorescence regime is not possible such as in OCT.

As EGFR is differentially expressed in the two cell lines used in this study, we made use of this differential expression of EGFR to regulate the amount of gold nanoparticles attached to the cells and thus elicit an optical contrast to "illuminate" the cancer cells over normal cells. This form of discrimination for a possible early cancer detection strategy is based solely on their molecular changes in biomarker expression rather than consequential phenotypic changes. The differences in reflectance intensity could potentially be detected by promising clinical optical modalities such as OCT or confocal endomicrosope working in the reflectance mode. In practice, the EGFR expression is detected at all stages of carcinogenesis, from normal-

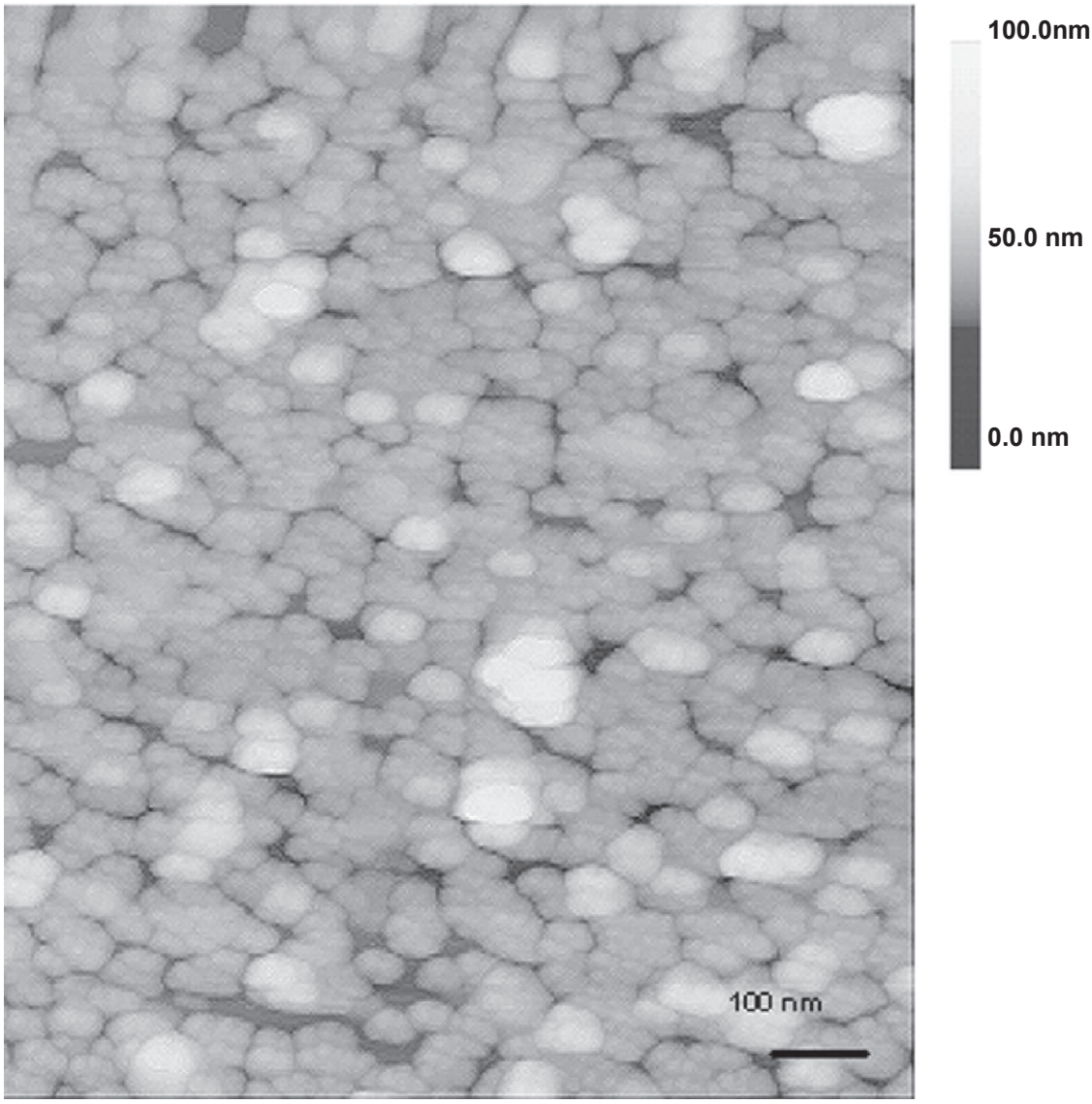

Figure 7 A 1 μm × 1 μm AFM image of the colloid film, showing closely-packed morphology of the gold nanoparticles in the film.

early hyperplasia, dysplasia to invasive carcinoma (Kannan et al 1994; Shintani et al 1996) and it is elevated during the progression from hyperplasia to dysplasia and increases during progression from dysplasia to invasive carcinoma (Shin et al 1994), thus giving a spectrum of expression levels with disease progression. As the reflectance signal depends on the level of EGFR expression, its intensity may further provide indications of the progression of diseases at the molecular level. However, we also observed heterogeneous labeling with the anti-EGFR gold nanoparticles on CNE2 cells (Figure 3c and 4d). This heterogeneity of protein expression in cell lines is common and has been described previously in the case of EGFR (Monaghan et al 1990). Therefore, further studies need to be conducted to quantitatively relate the reflectance signal from the gold nanoparticles attachment to the EGFR expression level in well-calibrated cell lines.

Although our in vitro results on cell lines seem promising, the use of gold nanoparticles in the same manner *in vivo* would warrant attention to the challenges in the way these nanoparticles could potentially elicit any body response and subsequently be eliminated from the body system with minimal side effects after their diagnostic use. Previous studies by other groups have shown that these gold nanoparticles tend to be taken up by the cells through endocytosis as fast as 1 h into the incubation with gold nanoparticles (Connor et al 2005). In this case, the anti-EGFR binding to cell surface EGFR could potentially provide a receptor-mediated endocytosis route for the gold nanoparticles. Connor and colleagues examined a series of gold nanoparticles for cellular

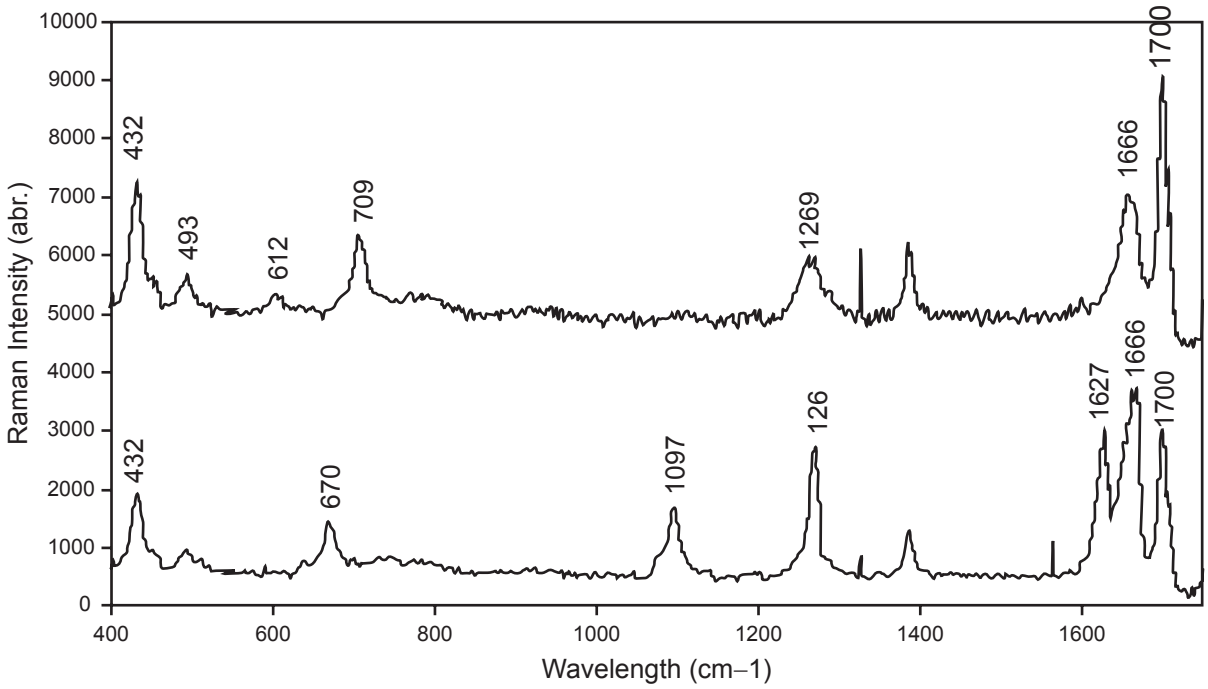

Figure 8 Typical SERS spectra of saliva samples collected from normal healthy individuals (top) and oral-cancer patients (bottom).

uptake and acute cytotoxicity in human leukemia cells and found that despite being taken up into the cells, spherical gold nanoparticles with a variety of surface modifiers were not inherently toxic to human cells (Connor et al 2005). Mukherjee et al have also shown that gold nanoparticles have no effect on gene expression or other global transcriptional pattern of human umbilical vein endothelial cells (HUVEC) (Mukherjee et al 2006).

Although tests on other forms of body response in terms of cellular adhesion effects, local biological effects or other systemic and remote effects have not been performed in this study, previous literatures have shown that colloidal gold nanoparticles is an inert material that can be injected to living animals without major complications. The small size of these particles enables them to extravasate out of the microcirculation easily and diffuse through the interstitial compartments of tissue efficiently. Without proper surface functionalization, most of the circulating nanoparticles will be trapped by reticuloendothelial system in liver, kidney, spleen and lungs and may remain there and in other tissue for a long time without interfering with metabolism of cells, although a small amount of gold nanoparticles may be secreted to the bile or urine (Eghtedari et al 2003). Whilst metal poisoning is often associated with renal and hepatic toxicities, Mukherjee and colleagues have determined the effect of gold nanoparticles administration on liver and renal function on mice and found that there were no significant differences between serum levels of creatinine, blood urea nitrogen, bilirubin alkaline phosphatase, alanine aminotransferase, and aspartate aminotransferase between gold nanoparticles treated and untreated control animals after 7 days of administration, thus concluding minimal effect of gold nanoparticles in renal and hepatic functioning (Mukherjee et al 2005). Despite the fact that gold nanoparticles have been injected to many patients in the past to treat rheumatoid arthritis or to study the function of reticuloendothelial system based on the past three decades of literature, there are only a few, if any, reports on complications of intravenous gold injection (Gumpel 1974).

Apart from enhancing the molecular contrast of cancer biomarkers under reflectance-mode imaging, gold nanoparticles can also be closely packed to form a film substrate to enhance the Raman signal of fluid analytes. Figure 5 illustrates the typical structures of a gold particle film fabricated using our deposition method. The detailed mechanism behind the formation of different regions in the deposited gold nanoparticle films is currently being studied. Nevertheless, we stress that the different types of colloid regions are readily discernible under the microscope, and it is easy to identify and avoid the non-uniform colloid layers during a SERS measurement. Measurements have also showed that uniform

films sized between 10 to 25 mm^2 can easily be reproduced using our current fabrication technique. A large colloid layer certainly has the advantage of ease of identification and localization under the microscope.

Figure 7 shows the typical AFM image of a uniformly coated region in the films. As observed from the figure, it is difficult to ascertain whether these islands are actually consisting of closely-spaced gold nanoparticles or large aggregates due to the fact that the gold nanoparticles are too small to be resolved by the AFM tip. However, it is possible to "artificially" enhance the spatial resolution by digitally processing the image using a band-pass filter as described previously (Micheletto et al 1995). From the processed image, the separation between two closest particle centers was estimated to be about 17 nm ± 15 %, which is comparable to the diameter of the individual particles. This result together with the double-peak feature seen in the UV-Vis spectrum in Figure 6 leads us to believe that the particles are closely-packed but physically separated. Thus, assuming a particle radius of 7.5 nm, the particle-to-particle separation of 17 nm can be translated to an interparticle distance of about 2 nm, which is close to the thickness of the adsorbed ion layer (0.5–1 nm) on the particle surface (Giersig and Mulvaney 1993), which in this case is the chloride ion. Note that in no case did we observe any interfering signal from this adsorbed ion layer.

The stability of the particle films was tested by immersing in a 10 % salt solution for 2 weeks. No re-suspension of particles was observed. There was also no re-suspension when saliva was applied on it. Such a good stability of the film is attributable to the strong electrostatic attraction between the negatively-charged particles and the underlying positively-charged SuperFrost®Plus surface. We stress that our films were assembled solely by the convection-induced particle flows in the wetting film near the contact line of the drying droplet and not by the spontaneous electrostatic adsorption of particles on the solid surface as in the case of electrostatic self-assembly (Sastry 2002). This was confirmed by immersing a SuperFrost®Plus glass slide in a colloidal solution of gold nanoparticles for 2 days. No particle attachment was observed. Furthermore, no stable colloid film can be formed if the gold suspension drop is dried on a normal microsope glass slide, which lacks the electrostatic layers. Films formed on these slides were either partially or completely removed upon rinsing with distilled water.

Typical SERS saliva spectra are shown in Figure 8. Three Raman peaks occurred at 670, 1079, and 1627 cm^{-1} are characteristic of saliva specimens collected from cancer patients. Of these bands, special note must be given to that situated at 1627 cm^{-1}, which were observed for 3 of the 5 saliva samples collected from the patients. This particular band was also observed in a previous Raman study of cancerous oral tissues (Ulas 1999). As to whether there is any correlation in the Raman signals at 1627 cm^{-1} between the saliva spectra and those derived from the tissues is not known at the moment. Certainly, a comparison of SERS saliva spectra and the Raman spectra derived from matched oral tissues should provide an answer. This is currently being carried out in our lab. We are also unable to evaluate the applicability of using the saliva spectrum for cancer staging at this stage, owing to insufficient samples. More samples are needed. The inconsistency of SERS has also been noted in this study. The signal reproducibility of our films is checked using Crystal Violet solution as test sample and found to be about 11% (data not shown). From further patient samples, we observe a sensitivity of the current technique in the range of around 70% ie,70% of the "abnormal" saliva shows abnormal peaks. However, none of the normal samples show these indicative peaks. We are currently working to develop a better SERS substrate consisting of periodic metallic nanostructures as opposed to the randomly-distributed nanoparticles film employed in the current study. This should improve signal reproducibility, thereby rendering quantitative analysis of the absolute signal intensity possible. However, the results of this study show the potential of these simple gold nanoparticles film for routine clinical diagnosis of oral cancer.

Conclusion

As cancer-associated biomarkers precede phenotypic manifestations of disease, there is a growing research interest in clinical molecular diagnostics for early cancer detection. Combining advances in biomedical optics and nanotechnology offers the opportunity to significantly impact future strategies towards the detection and diagnosis cancer. This study demonstrates the potential of antibody conjugated gold nanoparticles to target and illuminate cancer cells under a reflectance-based optical imaging system. In particular, we have shown that gold nanoparticles can provide an optical contrast to discriminate between cancerous and normal cells and their conjugation with antibodies also allows them to map the expression of relevant biomarkers for molecular imaging. Such molecular imaging has the potential to base disease detection on early molecular abnormalities before diseases become obvious with traditional imaging techniques. In addition, we have also demonstrated the use of SERS-active gold nanoparticle films fabricated using a simple drop-dry approach in the chemical analysis of saliva. SERS spectra of

saliva were obtained and shown to be differentiable between those acquired from normal individuals and oral cancer patients, thus showing promise of a simple SERS-based saliva assay for early diagnosis of oral cancer. All these may be translated to improved patient care by facilitating earlier cancer detection and phenotyping of tumors at a stage before debilitating or irreversible symptoms appear.

Acknowledgments

The authors would like to acknowledge the support from Division of Bioengineering, National University of Singapore through the award of a postgraduate research scholarship for JCY Kah. The authors would also like to thank the staff of the Tan Chin Tuan Laboratory of Optical Imaging and Photodynamic Therapy of Cancer, National Cancer Centre Singapore, where the work was carried out and Ms. Chan Yee Gek from Department of Anatomy, National University of Singapore for help with the TEM imaging as well as Dr. Sow Chorng Haur and Mr. Ong Peng Ming from the Department of Physics, National University of Singapore for their technical assistance on the AFM mapping.

References

Abrams MJ, Murrer BA. 1993. Metal compounds in therapy and diagnosis. *Science*, 261:725–30.

Bohren CF, Huffman DR. 1983. Absorption and Scattering of Light by Small Particles. New York: John Wiley and Sons.

Chen YC, Li TY, Tsai MF. 2002. Analysis of the saliva from patients with oral cancer by matrix-assisted laser desorption/ionization time-of-flight mass spectrometry. *Rapid Commun Mass Spectrom*, 16:364–9.

Connor EE, Mwamuka J, Gole A, et al. 2005. Gold nanoparticles are taken up by human cells but do not cause acute cytotoxicity. *Small*, 1:325–7.

Eghtedari MA, Copland JA, Popov YL, et al. 2003. Bioconjugated gold nanoparticles as a contrast agent for optoacoustic detection of small tumors. *Proc SPIE*, 4960:76–85.

Eisbruch A, Blick M, Lee JS, et al. 1987. Analysis of the epidermal growth factor receptor gene in fresh human head and neck tumors. *Cancer Res*, 47:3603–5.

El-Sayed IH, Huang X, El-Sayed MA. 2005. Surface plasmon resonance scattering and absorption of anti-EGFR antibody conjugated gold nanoparticles in cancer diagnostics: applications in oral cancer. *Nano Lett*, 5:829–34.

Geoghegan WD, Ackerman GA. 1977. Adsorption of horseradish peroxidase, ovomucoid, and anti-immunoglobulin to colloidal gold for the indirect detection of concanavalin A, wheat germ agglutinin, and goat anti-human immunoglobulin G on cell surfaces at the electron microscope level: a new method, theory, and application. *J Histochem Cytochem*, 25:1187–200.

Giersig M, Mulvaney P. 1993. Formation of ordered two dimensional gold colloid lattices by electrophoretic deposition. *J Phys Chem*, 97:6334–6.

Gumpel JM. 1974. The role of radiocolloids in the treatment of arthritis. *Rheumatol Rehabil*, 13:1–9.

Hayat MA. 1989. Colloidal Gold: Principles, Methods and Applications. New York: Academic Press.

Kannan S, Balaram P, Chandran GJ, et al. 1994. Co-expression of ras p21 and epidermal growth factor receptor during various stages of tumour progression in oral mucosa. *Tumour Biol*, 15:73–81.

Katherine C, Grabar R, Freeman G, et al. 1995. Preparation and characterization of Au colloid monolayers. *Anal Chem*, 67:735–43.

Ke LD, Adler-Storthz K, Clayman GL, et al. 1998. Differential expression of epidermal growth factor receptor in human head and neck cancers. *Head Neck*, 20:320–7.

Koenig F, Knittel J, Stepp H. 2001. Diagnosing cancer in vivo. *Science*, 292:1401–3.

Li XZ, Bai J, Lin J, et al . 2001. Serum fluorescence and Raman spectra for diagnosis of cancer. *Proc SPIE*, 4432:124–30.

Lumerman H, Freedman P, Kerpel S. 1995. Oral epithelial dysplasia and the development of invasive squamous cell carcinoma. *Oral Surg Oral Med Oral Pathol Oral Radiol Endod*, 79:321–9.

Micheletto R, Fukuda H, Ohtsu M, et al. 1995. A simple method for the production of a two-dimensional ordered array of small latex particles. *Langmuir*, 11:3333–6.

Monaghan P, Ormerod MG, O'Hare MJ. 1990. Epidermal growth factor receptors and EGF-responsiveness of the human breast-carcinoma cell line PMC42. *Int J Cancer*, 46:935–43.

Mukherjee P, Bhattacharya R, Wang P, et al. 2005. Antiangiogenic properties of gold nanoparticles. *Clin Cancer Res*, 11:3530–4.

Mukherjee P, Bhattacharya R, Patra CR, et al. 2006. Nanogold in Cancer Therapy and Diagnosis. In: Kumar CSSR (ed). Nanomaterials for Cancer Diagnosis, Nanotechnologies for the Life Sciences Book Series Vol. 7. 1st ed. Weinheim: WILEY-VCH Verlag GmbH and Co. KGaA. p 86–120.

Mulvaney P. 1996. Surface plasmon spectroscopy of nanosized metal particles. *Langmuir*, 12:788–800.

Murillo LE, Viera O, Vicuna E, et al. 2002. Growth kinetics of gold nanoparticles. *Comput Nanosci Nanotechnol*, 435–38.

Nouri AME, Thompson C, Cannell H, et al. 2000. Profile of epidermal growth factor receptor (EGFr) expression in human malignancies: Effects of exposure to EGF and its biological influence on established human tumor cell lines. *Int J Mol Med*, 6:495–500.

Sanchez-Gil J, Garcia-Ramos J, Mendez E. 2002. Electromagnetic mechanism in surface-enhanced Raman scattering from Gaussian-correlated randomly rough metal substrates. *Opt Express*, 10:879–86.

Sastry M. 2002. Assembling nanoparticles and biomacromolecules using electrostatic interactions. *Pure Appl Chem*, 74:1621–30.

Schultz S, Smith DR, Mock JJ, et al. 2000. Single-target molecule detection with nonbleaching multicolor optical immunolabels. *Proc Natl Acad Sci USA*, 97:996–1001.

Shin DM, Ro JY, Hong WK, et al. 1994. Dysregulation of epidermal growth factor receptor expression in premalignant lesions during head and neck tumorigenesis. *Cancer Res*, 54:3153–9.

Shintani S, Matsumura T, Alcalde RE, et al. 1996. Sequential expression of myc-, ras-, oncogene products and EGF receptor during DMBA-induced tongue carcinogenesis. *Int J Oncol*, 8:821–6.

Sokolov K, Aaron J, et al. 2003. Optical systems for in vivo molecular imaging of cancer. *Technol Cancer Res Treat*, 2:491–504.

Sokolov K, Follen M, Aaron J, et al. 2003. Real-time vital optical imaging of precancer using anti-epidermal growth factor receptor antibodies conjugated to gold nanoparticles. *Cancer Res*, 63:1999–2004.

Spafford MF, Koch WM, Reed AL, et al. 2001. Detection of Head and Neck Squamous Cell Carcinoma among exfoliated oral mucosal cells by microsatellite analysis. *Clin Cancer Res*, 7:607–12.

Taroni P, Pifferi A, Torricelli A, et al. 2003. In vivo absorption and scattering spectroscopy of biological tissues. *Photochem Photobiol Sci*, 2:124–9.

Ulas G. 1999. Laser Raman spectroscopy: some clinical applications. *Biomed Appl Lasers*, 77:101–7.

Wickline SA, Lanza GM. 2002. Molecular imaging, targeted therapeutics, and nanoscience. *J Cell Biochem Suppl*, 39:90–7.

Zheng W, Soo KC, Sivanandan R, et al. 2002. Detection of neoplasms in the oral cavity by digitized endoscopic imaging of 5-aminolevulinic acid-induced protoporphyrin IX fluorescence. *Int J Oncol*, 21:763–8.